Reactivity of the heteronuclear cluster Cp*IrOs$_3$(μ-H)$_2$(CO)$_{10}$ with some group 16 substrates

Padmamalini Srinivasan, Mei En Tai, Weng Kee Leong *

Department of Chemistry, National University of Singapore, Kent Ridge, Singapore 119260, Singapore

Abstract

The mixed metal cluster Cp*IrOs$_3$(μ-H)$_2$(CO)$_{10}$ (**1**) reacted readily with a number of group 16 substrates under chemical activation with TMNO. It reacted with C$_6$H$_5$SH to afford the novel cluster Cp*IrOs$_3$(μ-H)$_3$(CO)$_9$(μ-SPh) (**2**). It also reacted readily with Ph$_3$PSe to afford five new clusters, viz., Cp*IrOs$_3$(μ-H)$_2$(CO)$_9$(μ$_3$-Se) (**3**) Os$_3$(μ-H)$_2$(CO)$_7$(μ$_3$-Se)(PPh$_3$)$_2$ (**4**), Cp*IrOs$_3$(μ-H)$_2$(CO)$_9$(PPh$_3$) (**5**), Cp*Ir-Os$_3$(μ-H)$_2$(μ$_3$-Se)(CO)$_8$(PPh$_3$) (**6**) and Cp*IrOs$_3$(μ-H)$_2$(μ$_3$-Se)$_2$(CO)$_7$(PPh$_3$) (**7**). The reaction pathway for this reaction has been studied carefully and suggests that Ph$_3$PSe functioned primarily as a selenium atom transfer agent to give initially the even more reactive **3**. The reaction of **1** with di-*p*-tolyl ditelluride yielded three new clusters, **8–10**, which were non-interconverting stereoisomers with the formulation Cp*IrOs$_3$(μ-H)$_2$(μ-Te-*p*-C$_6$H$_4$CH$_3$)$_2$(CO)$_8$.
© 2005 Elsevier B.V. All rights reserved.

1. Introduction

Reasons for the continued interests in transition metal carbonyl clusters containing chalcogens include (a) the ability of the chalcogens to act as stabilizing ligands, thus preventing cluster fragmentation even under forcing reaction conditions [1], (b) the chalcogen, especially the heavier members, appear to be a key factor in cluster growth reactions [2], and (c) the unusual coordination modes and geometries they exhibit [3]. Much has been reported on the reactivity of homonuclear carbonyl clusters with group 16 substrates, but relatively little is known on the reactivity of mixed-metal clusters. We have recently initiated investigations into some osmium–iridium mixed-metal clusters containing cyclopentadienyl ligands [4]. In this paper, we would like to report our investigations into the reactivity of the cluster Cp*IrOs$_3$(μ-H)$_2$(CO)$_{10}$ (**1**) with

some group 16 substrates. We have chosen representatives from three different classes of group16 substrates to be examined, viz., a thiol, a phosphine selenide and a ditelluride.

2. Results and discussion

2.1. Reaction with thiophenol

Sulphur-containing clusters of the Group 8 and 9 metals are of interest as hydrodesulfurization catalysts [1b]. Thiols are known to react with homonuclear clusters via oxidative addition across the S–H bond [5]. Interestingly, the reaction involving the cluster Os$_3$(CO)$_{11}$(NCCH$_3$) has been reported to proceed via an intermediate with an agostic interaction [6]. In contrast, there appears to have been only one report on the reaction of a heteronuclear carbonyl cluster with thiols [7].

Reaction of **1** with thiophenol under chemical activation with trimethylamine *N*-oxide (TMNO) afforded bright orange crystalline Cp*IrOs$_3$(μ-H)$_3$(CO)$_9$(μ-SPh) (**2**).

---

* Corresponding author.
E-mail address: chmlwk@nus.edu.sg (W.K. Leong).

Cluster **2** has been characterized completely, including by a single crystal X-ray crystallographic analysis; the ORTEP plot together with selected bond parameters are shown in Fig. 1. Thus, the reaction involved oxidative addition of the thiol S–H bond via an Os–Os bond cleavage and a decarbonylation.

The molecular structure of **2** is that of a wingtip-bridged butterfly cluster; an osmium and the iridium atom occupy the hinge of the butterfly, and the benzene thiolate group bridges the wingtips. The $Os(3)\cdots Os(4)$ vector at 3.6970(8) Å is clearly non-bonding. There is a hydride bridging each of the three iridium–osmium edges. Bridging hydrides tend to elongate metal–metal bonds [8], and this is evident in the three iridium–osmium bond lengths [Ir(1)–Os(2) = 2.9037(3) Å, Ir(1)–Os(3) = 2.9242(3) Å, and Ir(1)–Os(4) = 2.9327(3) Å]. The thiolate bridge is unsymmetrical [Os(3)–S(5) = 2.4343(15) Å, Os(4)–S(5) = 2.4257(14) Å], but the bond parameters are similar to those in, for example, $HOs_3(\mu\text{-SMe})(\mu\text{-}\eta^2\text{-}C_6H_4)(CO)_9$ [2.418(4) and 2.433(5) Å] [9].

2.2. Reaction with triphenylphosphine selenide

The employment of tertiary phosphine selenides R_3PSe has been shown to be an effective method for synthesizing selenium-containing transition metal clusters. This method takes advantage of the frailty of the P=Se bond, which leads to its formal oxidative-addition onto the cluster, resulting in the transfer of the selenium atom [10].

The reaction of **1** with Ph_3PSe under TMNO activation proceeded at room temperature to afford up to four novel selenium-bridged osmium–iridium clusters, as depicted in Scheme 1. The cluster **5**, a phosphine-substituted derivative of **1**, has been reported earlier [4]. It moved together as one band on the TLC plate with cluster **4**, and had to be mechanically separated after crystallization; **4** and **5** appeared as orange-yellow and dark red crystals, respec-
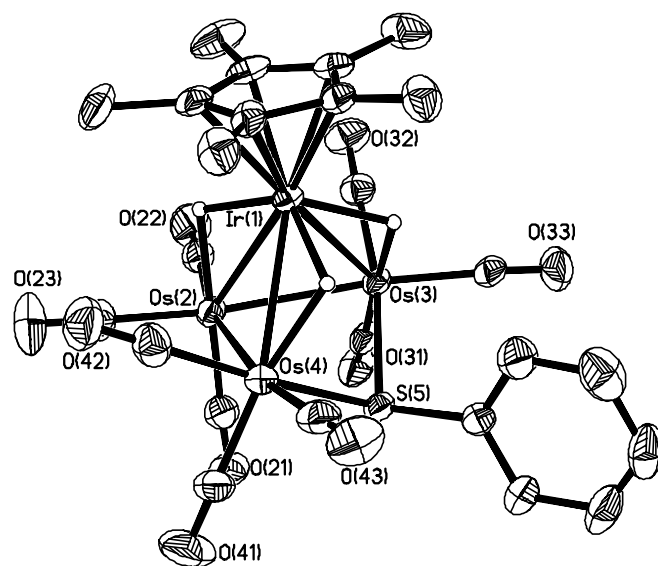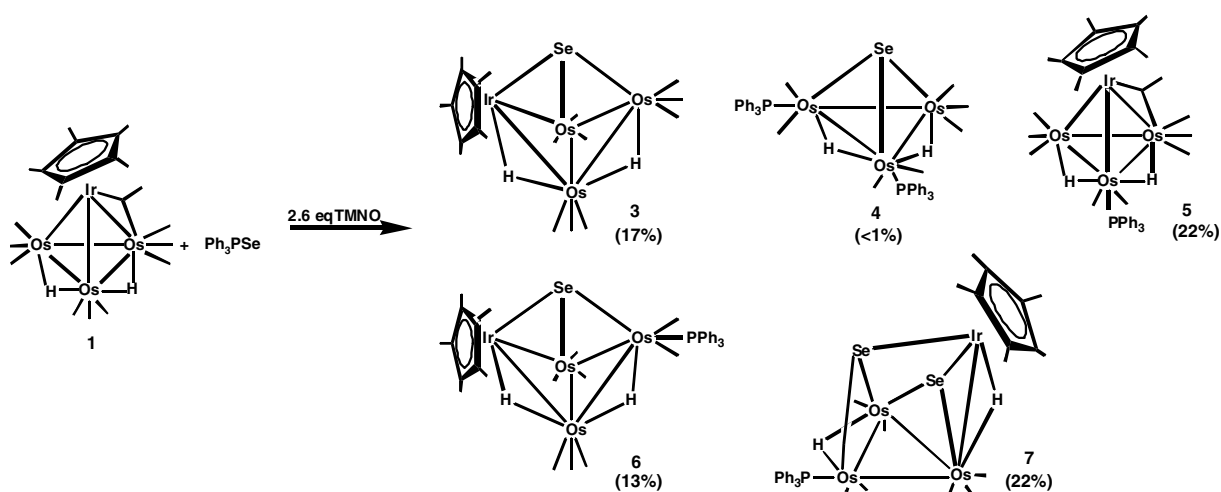

Fig. 1. ORTEP plot, with selected bond parameters, of **2**. Thermal ellipsoids are drawn at 50% probability level. Organic hydrogens are omitted for clarity. Ir(1)–Os(2) = 2.9037(3) Å; Ir(1)–Os(3) = 2.9242(3) Å; Ir(1)–Os(4) = 2.9327(3) Å; Os(2)–Os(3) = 2.8387(3) Å; Os(2)–Os(4) = 2.8448(3) Å; Os(3)–S(5) = 2.4343(15) Å; Os(4)–S(5) = 2.4257(14) Å; S(5)–Os(3)–Os(2) = 78.00(3)°; S(5)–Os(4)–Os(2) = 78.01°; Os(3)–Os(2)–Ir(1) = 61.213(7)°; Os(4)–Os(2)–Ir(1) = 61.340(7)°.

tively. All the novel compounds **3**, **4**, **6** and **7**, have been characterized, including by single crystal X-ray crystallographic analyses.

The ORTEP plots of **3** and **6** are given in Fig. 2, and common atomic numbering scheme and selected bond parameters for them are tabulated in Table 1. Cluster **6** is clearly a phosphine-substituted derivative of **3**. Their molecular structures comprise a butterfly tetrahedral core, with the iridium and an osmium atom making up the wingtips. The Se atom is triply bridging across the wingtips and one of the hinge Os atoms. The wing edges not spanned by the selenium are bridged by a hydride each; although the
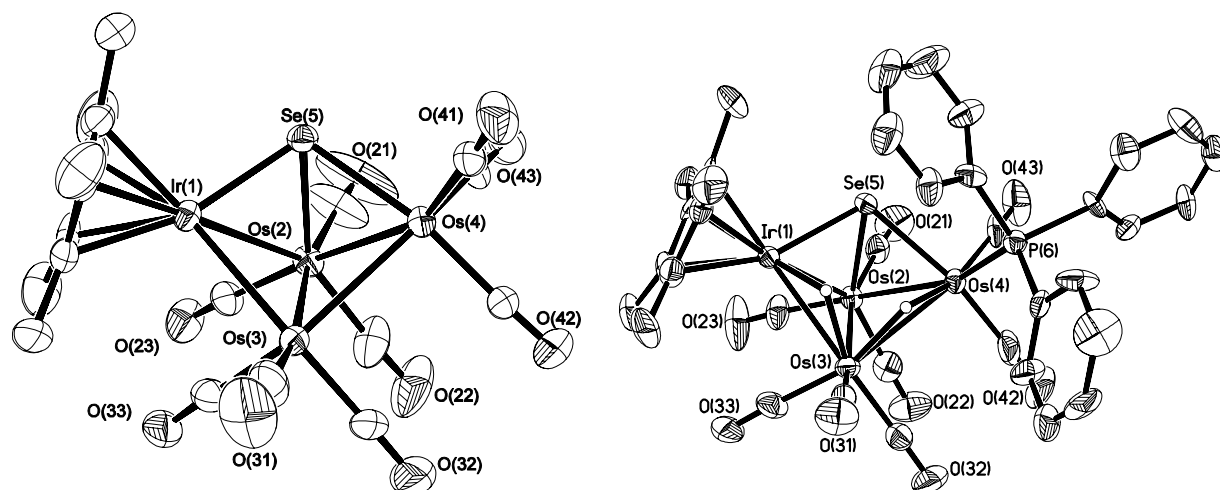

Scheme 1.

Fig. 2. ORTEP diagrams of **3** (left) and **6** (right). Thermal ellipsoids are drawn at 50% probability level. Organic hydrogens are omitted for clarity.

locations of these hydrides were placed by potential energy calculations [11], their positions are also corroborated by low angle electron density difference maps which show residual electron densities suggesting hydrides bridging those same edges. The ^{1}H NMR spectra are also consistent with these positions; that for **3** showing two doublets of equal intensities at δ −16.90 and −15.03 ppm ($^2J_{HH} = 3.3$ Hz), and that for **6** showing a doublet at δ −16.87 ppm ($^2J_{HH} = 3.3$ Hz) assignable to the hydride bridging the osmium–iridium bond, and a doublet of doublets at δ −13.95 ppm ($^2J_{PH} = 11.6$ Hz) assignable to the

hydride bridging an Os–Os bond. The interesting point here is that, quite contrary to expectations, the hydride bridging the Ir–Os bond in each structure does not bridge the longer of the two such bonds! In comparing the bond parameters between **3** and **6**, although some of their corresponding bond parameters are significantly different, there does not appear to be any discernible trend. A final point of interest is that the Os–P bond length in **6** is rather short.

The molecular structure of **4** is shown in Fig. 3, together with selected bond parameters. It is structurally similar to

Table 1
Common atomic numbering scheme and selected bond parameters for **3** and **6**

	3	**6**
L	CO	PPh$_3$
Bond length (Å)		
Ir–Os2	2.8927(5)	2.8512(7)
Ir–Os3	2.8163(5)	2.8395(7)
Os4–Os2	2.8123(5)	2.8135(7)
Os4–Os3	2.9484(5)	2.9812(7)
Os2–Os3	2.8477(5)	2.8489(7)
Ir–Se	2.4057(9)	2.4038(13)
Os4–Se	2.5242(9)	2.5100(13)
Os2–Se	2.5196(9)	2.5379(12)
Os4–L	–	2.316(3)
Bond angle (°)		
Os2–Ir–Os3	59.823(12)	60.082(7)
Os2–Os4–Os3	59.195(13)	58.811(17)
Dihedral angle between Os2Os3Ir and Os2Os3Os4	104.3	105.3

Fig. 3. ORTEP diagram of **4**. Thermal ellipsoids are drawn at 50% probability level. Organic hydrogens are omitted for clarity. Os(1)–Os(2) = 2.9858(4) Å; Os(1)–Os(3) = 2.7940(5) Å; Os(2)–Os(3) = 2.9419(4) Å; Os(1)–Se(4) = 2.4957(9) Å; Os(2)–Se(4) = 2.5042(9) Å; Os(3)–Se(4) = 2.5020(9) Å; Os(1)–P(1) = 2.334(2) Å; Os(2)–P(2) = 2.356(2) Å; Os(3)–Os(1)–Os(2) = 61.089(11)°; Os(3)–Os(2)–Os(1) = 56.236(10)°; Os(1)–Os(3)–Os(2) = 62.675(10)°.
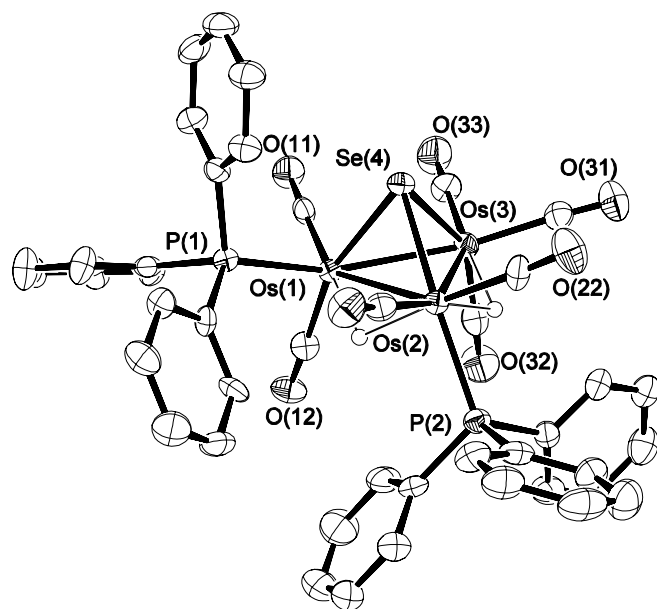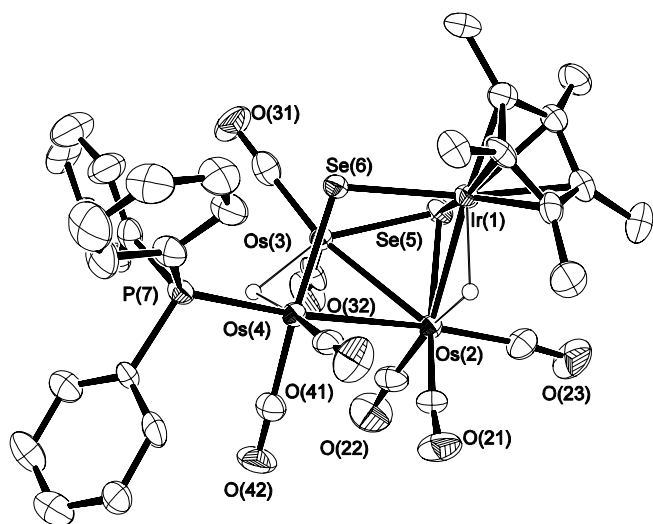
Fig. 4. ORTEP diagram of **7**. Thermal ellipsoids are drawn at 50% probability level. Organic hydrogens are omitted for clarity. Ir(1)–Os(2) = 2.9232(5) Å;   Os(2)–Os(3) = 2.9154(6) Å;   Os(2)–Os(4) = 3.0043(5) Å; Os(3)–Os(4) = 2.7423(5) Å;   Ir(1)–Se(5) = 2.4753(10) Å;   Ir(1)–Se(6) = 2.4967(10) Å; Os(2)–Se(5) = 2.5530(10) Å; Os(3)–Se(5) = 2.4674(10) Å; Os(3)–Se(6) = 2.5346(10) Å;   Os(4)–Se(6) = 2.5613(10) Å;   Os(4)–P(7) = 2.337(2) Å;   Os(3)–Os(2)–Ir(1) = 77.214(14)°;   Os(3)–Os(2)–Os(4) = 55.168(12)°;   Os(4)–Os(3)–Os(2) = 64.062(14)°;   Os(3)–Os(4)–Os(2) = 60.770(13)°.

that of the previously reported clusters Os$_3$(CO)$_9$(μ$_3$-Se)(PPh$_3$) (**4a**) and Os$_3$(μ-H)$_2$(CO)$_8$(μ$_3$-Se)(PPh$_3$) (**4b**) [10g]. Indeed, **4** is a further substituted analogue of **4b**, in which the additional phosphine (P(1)) occupies a pseudo-equatorial position on an adjacent osmium. As may be expected, the further substitution of a phosphine ligand has led to further elongation of the Os(1)–Os(2) bond that lies in between the two phosphines, although the two corresponding bonds in **4b** are rather unsymmetrical [2.9858(4) Å compared to 2.9440(4) and 2.9961(4) Å in **4** and **4b**, respectively]. In general, the bond lengths in **4** are slightly elongated with respect to those in **4b**, no doubt the result of increased electron density on the cluster framework from the additional phosphine.

The molecular structure of **7** is shown in Fig. 4, together with selected bond parameters. Its structure suggests that it may be regarded as derivable from **6** by the capping of the IrOs$_2$ wing with an additional μ$_3$-Se fragment. The Ir(1)···Os(3) vector is >3.6 Å, and hence is clearly non-bonding. The hydride positions as obtained from a potential energy calculation [11], were corroborated by a low angle electron density difference map and the ^{1}H NMR spectrum which showed a doublet at δ −12.10 ppm ($^2J_{PH}$ = 8.3 Hz) assignable to the hydride bridging the Os(3)–Os(4) edge, and a singlet at −18.72 assignable to that bridging the Ir(1)–Os(2) edge; no ^{1}H–^{1}H coupling was observable. The relatively small $^2J_{PH}$ value is also consistent with the hydride bridging the Os(3)–Os(4) edge which is *cis* to the phosphine, rather than the Os(2)–Os(4) edge which is *trans* to it. As in **3** and **6**, neither of the hydrides

bridge the longest edge [Os(2)–Os(4) = 3.0043(5) Å]; the lengthening of this bond is presumably in part due to *trans* influence of the PPh$_3$ ligand [P(7)–Os(4)–Os(2) = 173.39(6)°]. In fact, the Os(3)–Os(4) bond is remarkably short, even for an Os–Os bond not bridged by a hydride; it should be contrasted with the mean value of 2.877 Å in Os$_3$(CO)$_{12}$ [12], or the ∼2.84 Å in Os$_3$(CO)$_9$(μ-Se)$_2$ [13], although the reason for this is not clear. The four Os–Se bond lengths vary over a fairly wide range, from 2.4674(10) to 2.5613(10) Å (for Os(3)–Se(5) and Os(4)–Se(6), respectively).

We have carried out a series of reactions on **3**, **5** and **6** with PPh$_3$ and Ph$_3$PSe, both in the presence and the absence of TMNO, to determine how the various clusters **3**–**7** are related in the reaction pathway. Monitoring the original reaction of **1** by ^{1}H NMR spectroscopy showed that **3**–**7** were formed directly from the reaction. Formation of **5** evidently resulted from the reaction of free PPh$_3$ with **1** under TMNO activation [4]. The liberation of PPh$_3$ during the reaction was confirmed by both ^{31}P NMR spectroscopy and FAB MS, and also suggests that Ph$_3$PSe functioned primarily as a selenium transfer agent. This function was again evident when **5** in turn reacted with Ph$_3$PSe in the presence of TMNO to afford **6**. It is also in accord with our previous findings [10g]. We have found that **3** reacted with PPh$_3$ even in the absence of TMNO, to afford **4** and **6**, and forms **7** when reacted with Ph$_3$PSe under TMNO activation; these point to **3** as the precursor to **4**, **6** and **7**. Interestingly, **6** did not give rise to **7** either with PPh$_3$ or Ph$_3$PSe both in the presence or absence of TMNO. It was also found that a 1:2.6:2.6 ratio of **1**:TMNO:Ph$_3$PSe was required to ensure completion of reaction of **1**; reducing the ratio of TMNO or Ph$_3$PSe resulted in recovery of a large amount of unreacted **1**. This evidently points to the subsequent reactions of **3**, or the formation of **1**, being more rapid than the formation of **3** itself. We have thus proposed a reaction sequence as given in Scheme 2. The formation of **4** from **3** requires the loss of a Cp*IrCO fragment, although we do not know at this point what is the ultimate fate of this fragment. An example of such a cluster fragmentation with Ph$_3$PSe is that of the reaction of RuCo$_3$(μ-H)(CO)$_{12}$, which resulted in the loss of a Co fragment to give trinuclear clusters [10e].

2.3. Reaction with di-p-tolyl ditelluride

The chemistry of tellurium-containing clusters can be quite different from those of the sulphur or selenium analogues. For instance, the difference in reactivity of the trinuclear iron clusters, Fe$_3$(CO)$_9$(μ$_3$-E)$_2$, (E = S, Se, Te), towards Lewis bases has been attributed to the larger size of the Te atom which results in a more strained Fe–Te–Fe angle in Fe$_3$(CO)$_9$(μ$_3$-Te)$_2$ than in its sulphur and selenium analogues [14]. Nevertheless, reports on the reaction of clusters with diorganoditellurides appear to be scant [15]. The reaction of **1** with di-*p*-tolylditelluride at ambient tempera-
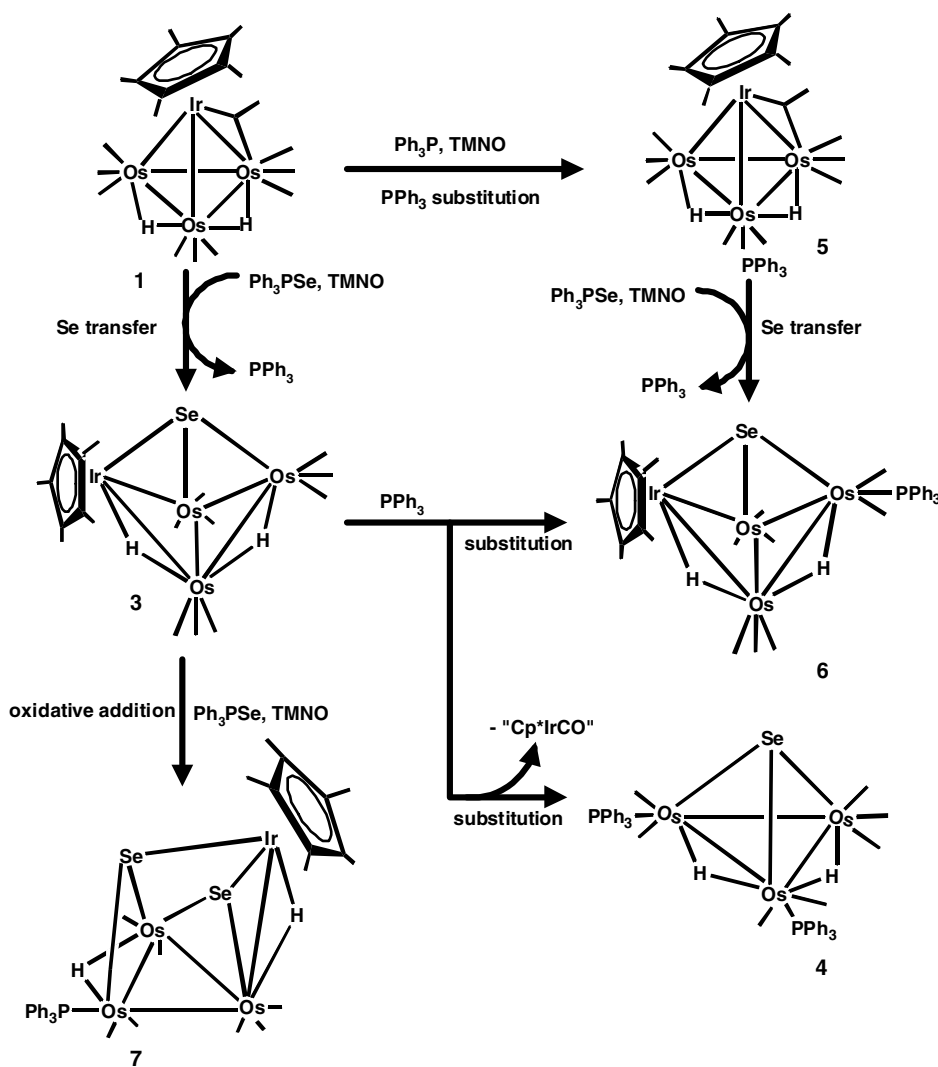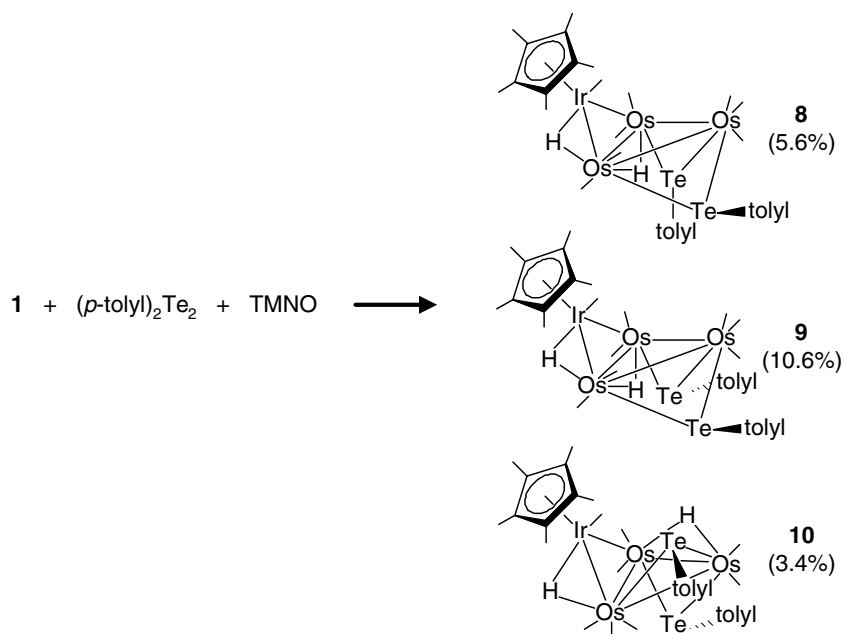
Scheme 2.

ture under chemical activation with TMNO afforded an orange-red solution which after chromatographic separation afforded three new compounds **8–10**, which were stereoisomers having the formulation, Cp*IrOs$_3$(μ-H)$_2$(μ-Te-p-C$_6$H$_4$CH$_3$)$_2$(CO)$_8$ (Scheme 3). All three have been characterized, including by single crystal X-ray crystallography, and their ORTEP plots are shown in Figs. 5–7, respectively.

Thus, the reaction of **1** with the diorganoditelluride is that of an oxidative addition reaction, upon decarbonylation with TMNO. The ^{1}H NMR spectrum of the crude reaction mixture showed the presence of all three isomers. Thus the products were not formed via decomposition on silica-gel plates, as has been observed in a related system [15a]. The ^{1}H NMR spectra of **8**, **9** and **10** showed two resonances each at high field, indicative of bridging metal hydrides. Two methyl signals each were observed for **8** and **10**, and one for **9**, consistent with their solid-state structures. The aromatic resonances for **8** were also partially assigned through selective decoupling experiment. Solutions of **8** and **9** (d_6-benzene) monitored by ^{1}H NMR

over a period of time at ambient temperature did not show any interconversion between the isomers; **10** was not sufficiently stable in solution over any appreciable period of time to allow a similar check on isomerization but its separation chromatographically alludes to a slow isomerization process, if any.

The crystal quality for **9** was, unfortunately, rather poor and the structure was modeled as exhibiting disorder of the heavy atom positions. Nevertheless the gross structural features are discernible. All three clusters have an open butterfly IrOs$_3$ metal core, with the iridium at one of the wingtips, and a telluride bridging each of the two Os–Os of the Os$_3$ wing. Besides the Cp*, the iridium also carries a carbonyl group. Clusters **8** and **9** are isomers differing in the relative orientation of the tolyl groups; in **8**, one of the tolyl is orientated away (*exo*) from the cluster core and the other inwards (*endo*), while in **9**, both tolyl groups are *exo*. Cluster **10** differs from **8** and **9** in that (a) one of the tellurium is oriented inwards towards the butterfly rather than away as in the others, (b) the wingtip osmium has only two instead

Scheme 3.
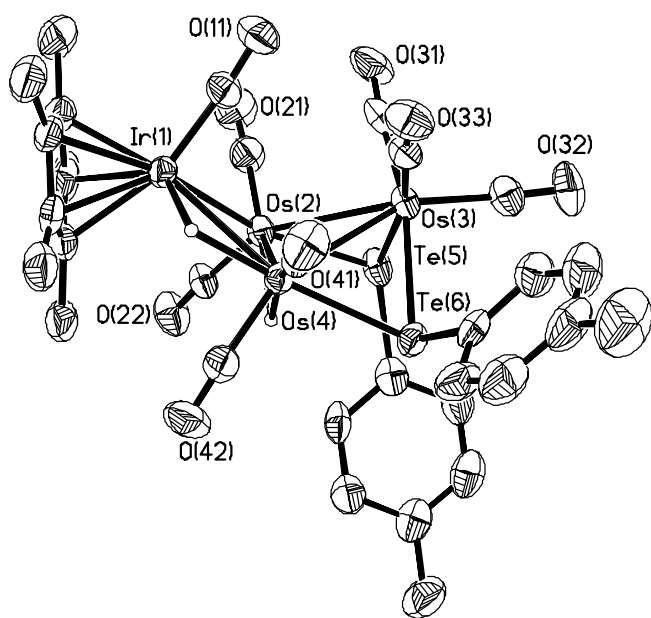
Fig. 5. ORTEP diagram of **8**. Thermal ellipsoids are drawn at 50% probability level. Organic hydrogens are omitted for clarity.
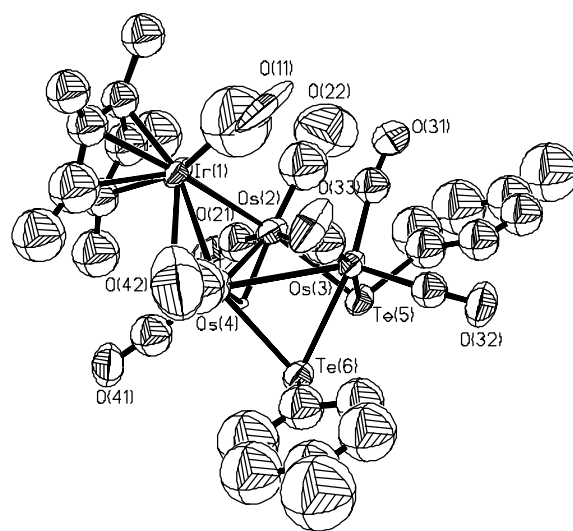
Fig. 6. ORTEP diagram of the major component of the disordered molecule of **9**. Thermal ellipsoids are drawn at 50% probability level. Organic hydrogens are omitted for clarity.

of three carbonyls, this third carbonyl being now located at one of the hinge osmiums, and (c) the positions of the hydrides. The positions of the hydrides were located by a potential energy calculation [11]. In the case of **8**, the positions are corroborated by a low angle electron density map. In **10**, the hydrides failed to show up in the electron density map, but the carbonyls along that edge [CO(32) and CO(42)] are bent away from each other, indicative of the steric influence of a hydride there. The disorder in **9** precluded reliable location of the hydrides, although potential

energy calculations indicated the positions given, which are also consistent with those in **8**. A common atomic numbering scheme, together with selected bond parameters, for **8**–**10** are tabulated in Table 2.

Strangely, as in **3**, **6** and **7**, the hydrides did not always bridge the longer metal–metal bonds. For instance, one of the hydrides bridges the shortest Os–Os bond in **8**, and the longest hinge bonds among the three clusters is that of **10** which is not bridged by an hydride. The longest metal–metal bonds are, in fact, bridged by a telluride. The bridging hydrides though, manifest themselves in the asym-
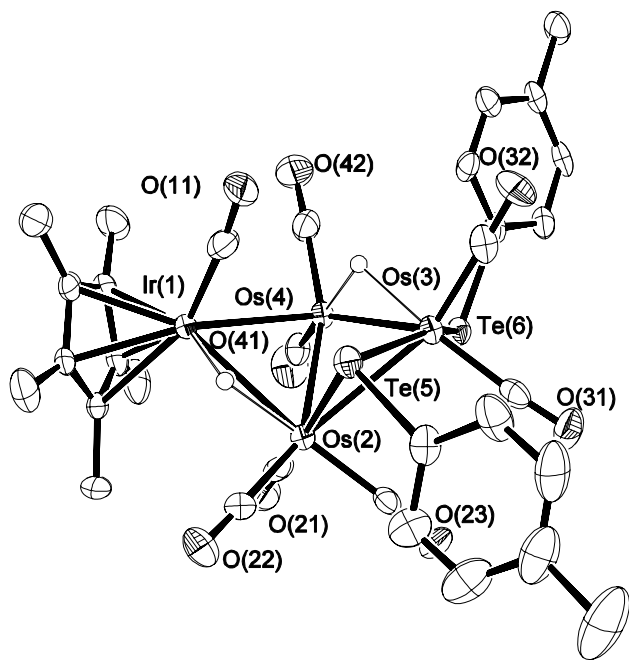
Fig. 7. ORTEP diagram of **10**. Thermal ellipsoids are drawn at 50% probability level. Organic hydrogens are omitted for clarity.

metry of the Ir–Os bond lengths. It may be expected that the unusual position of Te_6 in **10**, being on the *endo* face of t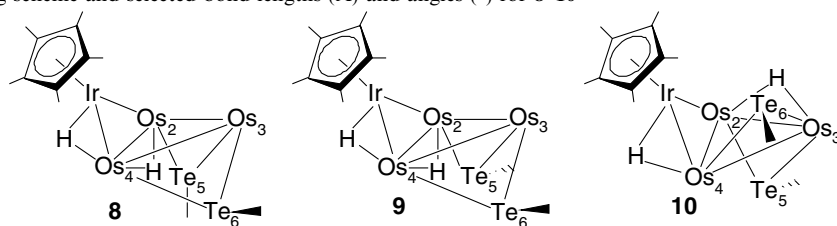he butterfly, would experience steric repulsion from the Cp*Ir moiety. Indeed this appears to be the case, the Os_4–Te_6 bond being significantly longer than the Os_3–Te_6 bond (2.7223(7) and 2.6180(7) Å, respectively) and quite unlike that for the other (*exo*) tellurium moieties which all appear to lean inwards. This steric effect is also evident in the increase in the dihedral angle between the $IrOs_2Os_4$ and $Os_2Os_3Os_4$ planes in **10** (127.7° as compared to 121.3° in **8**).

3. Concluding remarks

In this work, we have presented our findings on the reactivity of **1** with three classes of Group 16 substrates. Cluster **1** proved to be very reactive with these substrates under chemical activation, all reactions proceeding at ambient temperatures. With thiophenol and diorganoditelluride, **1** undergoes oxidative addition reactions. In the latter case, stereoisomers are obtained. With phosphine selenide, selenium atom transfer seems to be the initial step but the product so obtained is more reactive and quickly reacts further. One unusual structural feature in many of these products is the presence of very short metal–metal bonds, including some which are bridged by a hydride. It, therefore, seems certain that this class of reactions will turn up more unusual structures and reactivities to come.

Table 2
A common atomic numbering scheme and selected bond lengths (Å) and angles (°) for **8–10**

Compound	8	9[a]	10
Bond lengths (Å)			
Ir–Os₂	2.7519(5)	2.835(3)	2.7842(5)
Ir–Os₄	2.9299(4)	2.835(3)	2.9602(5)
Os₂–Os₃	2.9817(4)	2.983(2)	2.8274(5)
Os₃–Os₄	3.0086(4)	2.983(2)	2.9776(5)
Os₂–Os₄	2.7803(4)	2.810(4)	2.9188(5)
Os₂–Te₅	2.6149(7)	2.612(4)	2.6351(6)
Os₃–Te₅	2.7293(6)	2.699(3)	2.6385(7)
Os₃–Te₆	2.6927(6)	2.708(3)	2.6180(7)
Os₄–Te₆	2.6232(6)	2.618(3)	2.7223(7)
Bond angles (°)			
Os₂–Ir–Os₄	58.494(11)	59.41(7)	60.984(12)
Os₂–Os₃–Os₄	55.306(10)	56.18(7)	60.305(12)
Os₂–Te₅–Os₃	67.786(17)	68.32(8)	64.843(17)
Os₂–Te₆–Os₃	68.926(16)	68.12(8)	67.743(17)
Dihedral angles (°)			
IrOs₂Os₄ and Os₂Os₃Os₄	121.3	121.6	127.7
Os₂Os₃Os₄ and Os₂Os₃Te₅	128.9	121.3	122.8
Os₂Os₃Os₄ and Os₃Os₄Te₆	123.3	121.4	129.5
Os₂Os₃Te₅ and Os₃Os₄Te₆	91.5	97.8	131.8

[a] Disordered.

4. Experimental

All reactions were carried out using standard Schlenk techniques under an atmosphere of nitrogen. Solvents used in reactions were of AR grade, and were dried, distilled and kept under argon in flasks fitted with Teflon valves prior to use. The products were generally separated by thin-layer chromatography (TLC), using plates coated with silica gel 60 F254 of 0.25 mm or 0.5 mm thickness and extracted with hexane or dichloromethane. Infrared spectra were recorded as CH_2Cl_2 solutions unless otherwise stated on a Bio-Rad FTS 165 FTIR spectrometer at a resolution of 1 cm^{-1} using a solution cell with NaCl windows of path length 0.1 mm. NMR spectra were acquired on a Bruker ACF 300 MHz as $CDCl_3$ solutions unless otherwise stated. Selective decoupling experiments were carried out on a Bruker Avance DRX500 or Bruker AMX500 machine. Chemical shifts reported are referenced to residual protons of the solvent.

Mass spectra were collected using the fast atom bombardment (FAB) technique and were carried out on a Finnigan MAT95XL-T mass spectrometer normally with 3-nitrobenzyl alcohol matrix. Microanalyses were carried out by the microanalytical laboratory at the National University of Singapore. The cluster **1** [4], and di-*p*-tolyl ditelluride [16], were prepared according to published procedures. All other reagents were from commercial sources and used as supplied.

4.1. Reaction of 1 with thiophenol

To a 250 ml three necked flask containing **1** (30.0 mg, 0.0254 mmol) in dichloromethane (10 ml) was added excess thiophenol (4–5 drops). A solution of trimethylamine *N*-oxide (3.4 mg, 0.0304 mmol) in deoxygenated dichloromethane (20 ml) was then introduced dropwise via a pressure equalizing dropping funnel over a period of 2 h. The solution was stirred for a further 1 h. Removal of the solvent by rotary evaporation followed by chromatographic separation (6:4, v/v, hexane/dichloromethane) on silica gel TLC plates yielded a broad orange-red band of unreacted **1** (10 mg) and a second broad dark orange band of $Cp*IrOs_3(\mu-H)_3(CO)_9(\mu-SPh)$, **2** (18.7 mg, 58%).

IR (CH_2Cl_2): ν_{CO} 2072m, 2049vs, 2016s, 1989ms, 1968m, 1936mw,br cm^{-1}. ^1H NMR: δ 7.34–6.90 (m, 5H, Ph), 2.34 (s, 15H, Cp*), −15.58 (s, 2H, OsHIr), −16.60 (s, 1H, OsHIr). FAB-MS (*m/z*): 1261 [M$^+$]. Calc. for $C_{25}H_{23}IrO_9Os_3S$: C, 23.79; H, 1.84; S, 2.54. Found: C, 23.73; H, 2.17; S, 2.38%.

Diffraction quality crystals were grown from hexane and dichloromethane by slow diffusion.

4.2. Reaction of 1 with Ph₃PSe

In a typical reaction, to a solution of **1** (20.0 mg, 0.017 mmol) and Ph₃PSe (15.3 mg, 0.045 mmol) in CH_2Cl_2 (5 ml) was added a solution of TMNO (4.9 mg, 0.044 mmol) in CH_2Cl_2 (10 ml), and the mixture stirred for 1 h. Removal of the solvent by rotary evaporation followed by chromatographic separation on silica-gel TLC plates with hexane and dichloromethane (4:1, v/v) as eluant afforded, in order of elution, $Cp*IrOs_3(\mu-H)_2(CO)_9(\mu_3-Se)$, **3** (3.6 mg, 17%); unreacted **1** (2.3 mg); $Cp*IrOs_3(\mu-H)_2(CO)_9(PPh_3)$ (**5**) (5.2 mg, 22%, identified spectroscopically [4]); $Os_3(\mu-H)_2(CO)_7(\mu_3-Se)(PPh_3)_2$ (**4**) (0.1 mg, <1%); $Cp*IrOs_3(\mu-H)_2(\mu_3-Se)(CO)_8(PPh_3)$ (**6**) (3.2 mg, 13%); and $Cp*IrOs_3(\mu-H)_2(\mu_3-Se)_2(CO)_7(PPh_3)$ (**7**) (5.6 mg, 22%). Clusters **4** and **5** travelled as one band on the TLC plate and had to be mechanically separated after crystallization.

3: IR (hexane): ν_{CO} 2065vs, 2059vs, 2046m, 2024vs, 2008m, 2000m, 1989s, 1967w, 1950m cm^{-1}. ^1H NMR: δ 1.41 (s, 15H, Cp*), −15.03 (d, 1H, $^2J_{H-H} = 3.3$ Hz, OsHOs), −16.90 (d, 1H, IrHOs). FAB-MS (*m/z*): 1230.8 [M$^+$]. Calc. for $C_{19}H_{17}IrO_9Os_3Se$: C, 18.54; H, 1.39. Found: C, 18.70; H, 1.45%.

4: IR: ν_{CO} 2057s, 2038vs, 1991vs, 1976vs, 1956sh, 1923w cm^{-1}. ^1H NMR: δ 7.51–7.32 (m, 30H, Ph) −19.21 (dd, 1H, $^2J_{P-H} = 7.4$ Hz, 7.4 Hz, OsHOs), −19.30 (d, 1H, $^2J_{P-H} = 12.4$ Hz, OsHOs). $^{31}P\{^1H\}$ NMR: δ 1.22 (s), −4.55 (s). Hi-res MS (*m/z*): 1371.9658. Calc. for $C_{43}H_{32}P_2O_7$-$^{78}Se^{188}Os^{192}Os_2$: 1377.9585.

6: IR: ν_{CO} 2063m, 2019vs, 1996m, 1974sh, 1948w cm^{-1}. ^1H NMR: δ 7.56–7.42 (m, 15H, Ph), 1.59 (s, 15H, Cp*), −13.95 (dd, 1H, $^2J_{P-H} = 11.6$ Hz, $^2J_{H-H} = 3.3$ Hz, OsHOs), −16.87 (d, 1 H, IrHOs). $^{31}P\{^1H\}$ NMR: δ 5.05 (s). FAB-MS (*m/z*): 1465.35 [M$^+$]. Calc. for $C_{36}H_{32}IrO_8Os_3PSe$: C, 29.50; H, 2.20. Found: C, 29.70; H, 2.25%.

7: IR: ν_{CO} 2060vs, 2005sh, 1991vs, 1979sh, 1939w, 1910w cm^{-1}. ^1H NMR: δ 7.83–7.76 (m, 15H, Ph), 1.49 (s, 15H, Cp*), −12.10 (d, 1H, $^2J_{P-H} = 8.3$ Hz, OsHOs), −18.72 (s, 1H, IrHOs). $^{31}P\{^1H\}$ NMR: δ 12.30 (s). Hi-res MS (*m/z*): 1514.8425. Calc. for $C_{35}H_{29}O_7PIrSe_2$$^{188}Os^{190}$-$Os^{192}Os$: 1514.8414.

Diffraction-quality crystals for **3** were obtained from hexane solution by slow cooling, and by slow diffusion of hexane into a dichloromethane solution for **4**, **5** and **6**.

4.3. Reaction of 3 with PPh₃

To a solution of **3** (5 mg, 0.004 mmol) in dichloromethane (5 ml) was added PPh₃ (1.1 mg, 0.004 mmol) and the mixture stirred at room temperature for 3 h. Formation of **4** and **6** were verified by ^1H NMR spectroscopy.

4.4. Reaction of 3 with Ph₃PSe

To a solution of **3** (5 mg, 0.004 mmol) and Ph₃PSe (2.8 mg, 0.008 mmol) in dichloromethane was added dropwise a solution of TMNO (1.0 mg, 0.008 mmol) in

dichloromethane (10 ml) at room temperature. The mixture was stirred for 1 h. Formation of **7** was verified by ^{1}H NMR spectroscopy.

4.5. Reaction of 5 with Ph₃PSe

To a solution of **5** (5 mg, 0.003 mmol) and Ph₃PSe (1.2 mg, 0.003 mmol) in dichloromethane (10 ml) was added TMNO (0.4 mg, 0.003 mmol) and the reaction mixture stirred for 3 h. Formation of **6** was verified by ^{1}H NMR spectroscopy.

4.6. Reaction of 1 with di-p-tolyl ditelluride

To a 250 ml three-necked flask containing **1** (40.2 mg, 0.0356 mmol) in dichloromethane (10 ml) was added di-*p*-tolylditelluride (31.2 mg, 0.0711 mmol). A solution of trimethylamine *N*-oxide (8 mg, 0.07 mmol) in dichloromethane (20 ml) was deoxygenated and then introduced dropwise into the solution of **1** via a pressure equalizing dropping funnel over a period of 2 h. The solution was stirred for a further 1 h. Removal of the solvent by rotary evaporation followed by chromatographic separation (9:1, v/v, hexane/dichloromethane) on silica gel TLC plates yielded unreacted di-*p*-tolylditelluride ($R_f = 0.7$, trace amounts) identified from its ^{1}H NMR spectrum, unreacted **1** ($R_f = 0.65$, 3.5 mg) identified from its IR spectrum, an

orange solid of Cp*IrOs₃(μ-H)₂(μ-Te-*p*-C₆H₄CH₃)₂(CO)₈ (**8**) ($R_f = 0.57$, 3.0 mg, 5.6%), a dark orange solid of **9** ($R_f = 0.53$, 5.6 mg, 10.6%), and pink crystals of **10** ($R_f = 0.15$, 1.8 mg, 3.4%).

8: IR: ν_{CO} 2057s, 2009s, 1997vs, 1980m, 1960m, 1936ms, 1904m cm^{-1}. ^{1}H NMR (C₆D₆): δ 7.41 (d, 2H, $^3J_{H-H} = 7.85$ Hz, C₆H$_{2b}$H$_{2b'}$CH₃), 7.30 (d, 2H, $^3J_{H-H} = 7.85$ Hz, C₆H$_{2a}$H$_{2a'}$CH₃), 6.59 (d, 2H, C₆H$_{2b}$H$_{2b'}$CH₃), 6.58 (d, 2H, C₆H$_{2a}$H$_{2a'}$CH₃), 2.04 (s, 15H, Cp*), 1.93 (s, 3H, CH₃), 1.85 (s, 3H, CH₃), −12.83 (s, 1H, MHM); −13.38 (s, 1H, MHM). FAB-MS (*m/z*): 1561.1 [M$^+$]. Calc. for C₃₂H₃₁Ir-O₈Os₃Te₂. 1/4C₆H₁₄: C, 25.41; H, 2.19. Found: C, 25.37; H, 2.00%. Presence of hexane was confirmed by ^{1}H NMR spectroscopy.

9: IR: ν_{CO} 2058s, 2010s, 1997s, 1979m, 1960m, 1937ms, 1906m cm^{-1}. ^{1}H NMR (C₆D₆): δ 7.57 (d, 4H, $J_{H-H} = 7.4$ Hz, C₆H₄CH₃), 6.73 (d, 4H, $J_{H-H} = 8.3$ Hz, C₆H₄CH₃), 2.01 (s, 15H, Cp*), 1.93 (s, 6H, 2 × Me), −13.16 (s, 1H, MHM); −15.11 (s, 1H, MHM). FAB-MS (*m/z*): 1564.1 [M$^+$]. Calc. for C₃₂H₃₁IrO₈Os₃Te₂: C, 24.61; H, 2.00. Found: C, 24.51; H, 2.48%.

10: IR: ν_{CO} 2063ms, 2040mw, 2026vs, 2012ms, 1982m, 1958m cm^{-1}. ^{1}H NMR (C₆D₆): δ 7.71 (d, 2H, $^3J_{H-H} = 8.2$ Hz, C₆H$_{2a}$H$_{2a'}$CH₃), 7.57 (d, 2H, C₆H$_{2a}$H$_{2a'}$CH₃), 6.83 (d, 2H, $^3J_{H-H} = 7.4$ Hz, C₆H$_{2b}$H$_{2b'}$CH₃), 6.77 (d, 2H, C₆H$_{2b}$H$_{2b'}$CH₃), 1.68 (s, Cp*), 1.99 (s, 3H, CH₃), 1.96 (s, 3H, CH₃); −18.45 (s, 1H, MHM); −20.42 (s, 1H,

Table 3
Crystal and structure refinement data for compounds **3**, **4**, **6** and **7**

Compound	**3**	**4**	**6**	**7**
Empirical formula	C₁₉H₁₇IrO₉Os₃Se	C₄₃H₃₂O₇Os₃P₂Se	C₃₆H₃₂IrO₈Os₃PSe	C₃₅H₃₂IrO₇Os₃PSe₂
Formula weight	1231.09	1372.19	1465.35	1516.30
Crystal system	Monoclinic	Monoclinic	Triclinic	Triclinic
Space group	$P2_1/n$	$P2_1$	$P\bar{1}$	$P\bar{1}$
Unit cell dimensions				
a (Å)	8.9022(2)	9.0916(3)	11.4938(7)	10.0835(6)
b (Å)	19.5490(4)	20.8054(8)	11.8348(7)	10.3971(6)
c (Å)	14.5565(3)	11.5487(4)	16.9070(9)	18.6602(11)
α (°)	90	90	105.050(1)	78.9320(10)
β (°)	93.829(1)	110.120(2)	94.426(1)	84.8280(10)
γ (°)	90	90	118.879(1)	89.6690(10)
Volume (Å³)	2527.60(9)	2051.18(13)	1888.10(19)	1911.98(19)
Z	4	2	2	2
Density (calculated) (Mg/m³)	3.235	2.222	2.577	2.634
Absorption coefficient (mm^{-1})	21.765	10.284	14.630	15.396
$F(000)$	2168	1276	1332	1372
Crystal size (mm³)	0.34 × 0.14 × 0.14	0.36 × 0.36 × 0.34	0.20 × 0.04 × 0.04	0.22 × 0.12 × 0.07
Theta range for data collection (°)	2.08–26.37	2.12–30.01	2.04–26.37	2.03–26.37
Reflections collected	24978	18676	27586	24491
Independent reflections [R_{int}]	5161 [0.0350]	10265 [0.0356]	7720 [0.0620]	7814 [0.0476]
Maximum and minimum transmission	0.151 and 0.051	0.128 and 0.119	0.592 and 0.158	0.412 and 0.133
Data/restraints/parameters	5161/0/303	10265/1/505	7720/0/456	7814/0/447
Goodness-of-fit on F^2	1.207	1.036	1.234	1.044
Final R indices [$I > 2\sigma(I)$]	$R_1 = 0.0358$, $wR_2 = 0.0723$	$R_1 = 0.0383$, $wR_2 = 0.0867$	$R_1 = 0.0551$, $wR_2 = 0.1021$	$R_1 = 0.0390$, $wR_2 = 0.0841$
R indices (all data)	$R_1 = 0.0381$, $wR_2 = 0.0733$	$R_1 = 0.0422$, $wR_2 = 0.0889$	$R_1 = 0.0650$, $wR_2 = 0.1062$	$R_1 = 0.0520$, $wR_2 = 0.0971$
Absolute structure	–	0.037(9)	–	–
Largest difference in peak and hole (e Å^{-3})	1.529 and −0.995	3.466 and −1.354	1.484 and −1.769	1.712 and −1.379

Table 4
Crystal and structure refinement data for compounds **2**, **8**–**10**

Compound	2	8	9	10
Empirical formula	$C_{25}H_{23}IrO_9Os_3S$	$C_{33.50}H_{34.50}IrO_8Os_3Te_2$	$C_{32}H_{31}IrO_8Os_3Te_2$	$C_{32}H_{31}IrO_8Os_3Te_2$
Formula weight	1262.29	1583.11	1561.57	1561.57
Crystal system	Monoclinic	Monoclinic	Trigonal	Monoclinic
Space group	$P2_1/n$	$P2_1/n$	$P31c$	$P2_1/c$
Unit cell dimensions				
a (Å)	9.8007(2)	14.3405(5)	17.5141(6)	8.5464(4)
b (Å)	16.8974(4)	17.5501(7)	17.5141(6)	17.8810(8)
c (Å)	17.8438(4)	17.4210(6)	24.8205(16)	23.6636(10)
α (°)	90	90	90	90
β (°)	94.8210(10)	112.1920(10)	90	90.533(1)
γ (°)	90	90	120	90
Volume (Å^3)	2944.59(11)	4059.7(3)	6593.5(5)	3616.1(3)
Z	4	4	6	4
Density (calculated) (Mg/m^3)	2.847	2.590	2.360	2.868
Absorption coefficient	17.527	14.079	13.001	15.804
$F(000)$	2264	2834	4176	2784
Crystal size (mm^3)	$0.34 \times 0.26 \times 0.22$	$0.30 \times 0.18 \times 0.16$	$0.24 \times 0.08 \times 0.06$	$0.20 \times 0.14 \times 0.10$
Theta range for data collection (°)	2.29–30.02	2.32–30.03	2.12–26.36	2.06–29.61
Reflections collected	14495	41835	89766	30870
Independent reflections [R_{int}]	8403 [0.0345]	11552 [0.0444]	8967 [0.1450]	9344 [0.0606]
Maximum and minimum transmission	0.113 and 0.066	0.212 and 0.101	0.509 and 0.146	0.301 and 0.144
Data/restraints/parameters	8403/0/357	11552/0/453	8967/57/233	9344/0/422
Goodness-of-fit on F^2	1.071	1.084	1.114	1.024
Final R indices [$I > 2\sigma(I)$]	$R_1 = 0.0300$, $wR_2 = 0.0641$	$R_1 = 0.0460$, $wR_2 = 0.0982$	$R_1 = 0.0816$, $wR_2 = 0.1629$	$R_1 = 0.0439$, $wR_2 = 0.0867$
R indices (all data)	$R_1 = 0.0394$, $wR_2 = 0.0668$	$R_1 = 0.0630$, $wR_2 = 0.1058$	$R_1 = 0.1377$, $wR_2 = 0.1869$	$R_1 = 0.0669$, $wR_2 = 0.0941$
Largest difference in peak and hole (e Å^{-3})	1.612 and −0.960	2.569 and −1.066	2.452 and −1.143	2.186 and −1.130

MHM). Hi-res MS (*m/z*): 1561.8530. Calc. for $C_{32}H_{31}O_8{}^{191}Ir^{128}TeTe^{188}Os^{190}OsOs$: 1561.8526.

4.7. X-ray crystal structure determinations

Crystals were mounted on quartz fibres. X-ray data were collected on a Bruker AXS APEX system, using Mo Kα radiation, at 223 K with the SMART suite of programs [17]. Data were processed and corrected for Lorentz and polarization effects with SAINT [18], and for absorption effects with SADABS [19]. Structural solution and refinement were carried out with the SHELXTL suite of programs [20]. Crystal and refinement data are summarized in Tables 3 and 4.

The structures were solved by direct methods to locate the heavy atoms, followed by difference maps for the light, non-hydrogen atoms. With the exception of one hydride in **9** which was located in a low angle difference map, the hydrides were placed by potential energy calculations with the program XHYDEX [11], given fixed isotropic thermal parameters, and refined riding on one of the osmium atoms they are attached to. All non-hydrogen atoms were generally given anisotropic displacement parameters in the final model, except for **9**. Organic hydrogen atoms were placed in calculated positions and refined with a riding model.

Cluster **9** was refined as a racemic twin, and the structure also exhibited disorder of the heavy atoms, which was modeled with another alternative orientation for an OsTe$_2$ fragment. Appropriate restraints were placed to keep the refinement stable.

Appendix A. Supplementary data

Experimental details of additional reactions involving **1** and Ph$_3$PSe. Crystallographic data (excluding structure factors) for the structures in this paper have been deposited with the Cambridge Crystallographic Data Centre as supplementary publication numbers CCDC 285088–285095. Copies of the data can be obtained, free of charge, on application to CCDC, 12 Union Road, Cambridge CB2 1EZ, UK, fax: +44 1223 336 033 or e-mail: deposit@ccdc.cam.ac.uk. Supplementary data associated with this article can be found, in the online version, at doi:10.1016/j.jorganchem.2005.10.037.

References

[1] (a) J. Mizutani, K. Matsumoto, Chem. Lett. (2000) 72;
(b) B.C. Wiegand, C.M. Friend, Chem. Rev. 92 (1992) 491.

[2] For examples, see (a) M. Shieh, S.-F. Lin, Y.-W. Guo, M.-H. Hsu, Y.-W. Lai, Organometallics 23 (2004) 5182;
(b) M. Brandl, H. Brunner, H. Cattey, Y. Mugnier, J. Wachter, M. Zabel, J. Organomet. Chem. 659 (2002) 22;
(c) H. Brunner, D. Lucas, T. Monzon, Y. Mugnier, B. Nuber, B. Stubenhofer, A.C. Stuckl, J. Wachter, R. Wanninger, M. Zabel, Chem. Eur. J. 6 (2000) 493;
(d) S.W.A. Fong, T.S.A. Hor, J. Chem. Soc., Dalton Trans. (1999) 639;
(e) P. Mathur, R. Trivedi, P. Sekar, D. Chakrabarty, M.M. Hossain, V.G. Puranik, J. Cluster Sci. 7 (1996) 191;
(f) P. Mathur, P. Sekar, J. Chem. Soc., Chem. Commun. (1996) 727;
(g) R.E. Bachman, K.H. Whitmire, J. van Hal, Organometallics 14 (1995) 1792;
(h) M. Shieh, T.-F. Tang, S.-M. Peng, G.-H. Lee, Inorg. Chem. 34 (1995) 2797;
(i) I.L. Eremenko, S. Nefedov, H. Berke, B.I. Kolobkov, V.M. Novotortsev, Organometallics 14 (1995) 1132;
(j) V.W. Day, D.A. Lesch, T.B. Rauchfuss, J. Am. Chem. Soc. 104 (1982) 1290.
[3] (a) P. Braunstein, L.A. Oro, P.R. Raithby, Metal Clusters in Chemistry, Wiley–VCH, Weinheim, New York, 1999;
(b) M.L. Steigerwald, T. Siegrist, E.M. Gyorgy, B. Hessen, Y.U. Kwon, S.M. Tanzler, Inorg. Chem. 33 (1994) 3389.
[4] P. Srinivasan, W.K. Leong, J. Organomet. Chem. (accepted)..
[5] For example (a) S.M.T. Abedin, K.A. Azam, M.B. Hursthouse, S.E. Kabir, K.M.A. Malik, M.A. Mottalib, E. Rosenberg, J. Cluster Sci. 12 (2001) 5;
(b) H. Egold, D. Schwarze, U. Florke, J. Chem. Soc., Dalton Trans. (1999) 3203;
(c) P. Braunstein, J.R. Galsworthy, B.J. Hendan, H.C. Marsmann, J. Organomet. Chem. 551 (1998) 125;
(d) M.C. Jennings, R. Puddephatt, J. Inorg. Chem. 27 (1988) 4280;
(e) E.G. Bryan, B.F.G. Johnson, J. Lewis, J. Chem. Soc., Dalton Trans. (1977) 1328.
[6] K. Kiriakidou, M.R. Plutino, F. Prestopino, M. Johansson, L.I. Elding, E. Nordlander, F. Prestopino, M. Monari, E. Valls, R. Gobetto, S. Aime, Chem. Commun. (1998) 2721.
[7] S. Jaeaeskelaeinen, J. Pursiainen, T.A. Pakkanen, J. Organomet. Chem. 487 (1995) 197.
[8] (a) M.R. Churchill, B.G. DeBoer, F. Rotella, J. Inorg. Chem. 15 (1976) 1843;

(b) R. Bau, R.G. Teller, S.W. Kirtley, T.F. Koetzle, Acc. Chem. Res. 12 (1979) 176.
[9] R.D. Adams, D.A. Katahira, L.W. Yang, Organometallics 1 (1982) 235.
[10] (a) D. Cauzzi, C. Graiff, R. Pattacini, G. Predieri, A. Tiripicchio, S. Kahlal, J.-Y. Saillard, Eur. J. Inorg. Chem (2004) 1063;
(b) C. Graiff, G. Predieri, A. Tiripicchio, Eur. J. Inorg. Chem. (2003) 1659;
(c) D. Belletti, D. Cauzzi, C. Graiff, A. Minarelli, R. Pattacini, G. Predieri, A. Tiripicchio, J. Chem. Soc., Dalton Trans. (2002) 3160;
(d) C. Graiff, A. Ienco, C. Massera, C. Mealli, G. Predieri, A. Tiripicchio, F. Ugozzoli, Inorg. Chim. Acta 330 (2002) 95;
(e) P. Braunstein, C. Graiff, C. Massera, G. Predieri, J. Rose, A. Tiripicchio, Inorg. Chem. 41 (2002) 1372;
(f) D. Cauzzi, C. Graiff, C. Massera, G. Predieri, A. Tiripichio, J. Cluster Sci 12 (2001) 259;
(g) W.K. Leong, W.L.J. Leong, J. Zhang, J. Chem. Soc., Dalton Trans. (2001) 1087;
(h) D. Cauzzi, C. Graiff, M. Lanfranchi, G. Predieri, A. Tiripicchio, J. Chem. Soc., Dalton Trans. (1995) 2321.
[11] A.G. Orpen, XHYDEX, School of Chemistry, University of Bristol, UK, 1997.
[12] M.R. Churchill, B.G. DeBoer, Inorg. Chem. 16 (1977) 878.
[13] B.F.G. Johnson, J. Lewis, P.G. Lodge, P.R. Raithby, Acta Crystallogr., Sect. B B37 (1981) 1731.
[14] D.A. Lesch, T.B. Rauchfuss, Organometallics 1 (1982) 499.
[15] (a) For examples, see J. Zhang, W.K. Leong, J. Chem. Soc., Dalton Trans. (2000) 1249;
(b) A.A. Pasynskii, Yu.V. Torubaev, K.A. Lysenko, A.Yu. Lyakina, Zh.V. Dobrokhotova, V.M. Novotortsev, Zh. Neorg. Khim. 43 (1998) 939.
[16] N. Petragnani, Tellurium in Organic Synthesis, Academic, London, 1994.
[17] SMART version 5.628, Bruker AXS Inc., Madison, Wisconsin, USA, 2001.
[18] SAINT+ version 6.22a, Bruker AXS Inc., Madison, Wisconsin, USA, 2001.
[19] G.M. Sheldrick, SADABS, 1996.
[20] SHELXTL version 5.1, Bruker AXS Inc., Madison, Wisconsin, USA, 1997.